Statistical Determination of Cracking Probability for Mass Concrete

Kyle A. Riding, P.E., M.ASCE[1]; Jonathan L. Poole, P.E., M.ASCE[2]; Anton K. Schindler, P.E., M.ASCE[3]; Maria C. G. Juenger[4]; and Kevin J. Folliard[5]

Abstract: This study addresses the use of a stress-to-strength ratio as a failure criterion for thermal cracking. Restrained cracking frame specimens and accompanying match-cured concrete cylinders were tested to determine the ratio of stress-to-splitting tensile strength at cracking. A stress-to-splitting tensile strength ratio of 0.57 was found to give a 50% probability of cracking and lognormal standard deviation of 0.16 when splitting tensile cylinders sized 100 × 200 mm (4 × 8 in.) and 150 × 150 mm (6 × 6 in.) rigid cracking frame specimens were used to determine the stress at cracking. Lognormal fits of the cracking stress from 64 cracking frame tests and the tensile strength calculated from the measured compressive strength using three commonly used equations based on compressive strength were developed.
DOI: 10.1061/(ASCE)MT.1943-5533.0000947.

Author keywords: Cracking risk; Thermal stress; Tensile strength.

Introduction

Cementitious materials release heat during the early stages of the hydration reactions. As a result, large concrete members can develop very high interior temperatures during curing, while the exterior can be closer to ambient temperature. The lack of uniform temperature, modulus of elasticity development, and restraint of the concrete member can create large internal stresses, as specified by the American Concrete Institute (ACI) (2007). These internal stresses, when high enough relative to its ultimate tensile strength, can cause cracking in the concrete member, which may reduce the structure's intended service life or, when severe enough, be a structural concern.

In recent years, specifications have begun requiring contractors and material suppliers to consider thermal cracking when engineering concrete mixture proportions, designing formwork, and planning construction sequences. Several methods of varying complexity have been proposed for estimating the cracking risk of concrete members (ACI 2007; Gajda and VanGeem 2002; Rostásy et al. 1998; Emborg 1998a; Kanda et al. 2008). Although there are many methods of estimating the cracking potential of a concrete member such as strain capacity, the cracking potential is often defined as the ratio between the stress and strength as shown in Eq. (1) (Emborg 1998a; Kanda et al. 2008)

$$\eta^{\max} = \left[\frac{\sigma_t(t)}{f^*_{ct}(t)}\right]^{\max} \tag{1}$$

where $\eta^{\max}$ is the maximum cracking potential in the member during the analysis period, σ_t is the tensile stress (MPa) in the member at a time t (h), and f^*_{ct} is the tensile strength of the member (MPa) at time t. Since there is an inherent uncertainty to the stress and strength as measured, none of the values in Eq. (1) is discrete. Instead, normal distributions of stress and strength are usually assumed in probabilistic models of concrete, as shown in Fig. 1 (van Breugel and Lokhorst 2001). The overlap between the stress and strength probability density functions defines the cracking probability. The mean and standard deviation of the concrete strength and stress are needed to estimate the cracking probability (Eberhardt et al. 1994; van Breugel and Lokhorst 2001). Because the variability of the stress at cracking in restrained cracking tests is unknown and would require many costly experiments to determine, an alternative method for determining the cracking probability developed from experimental results instead of analytical results (Kanda et al. 2008) would benefit thermal stress analysis. This method is based on the fact that it is not necessary to determine the probability distribution of the stress and strength individually if the probability distribution of the composite stress-to-strength ratio in a stress analysis is known.

In order to determine cracking probability using Eq. (1), one must know the strength and stress probability density functions. The tensile strength of concrete is most commonly and practically measured using the concrete splitting tensile test (ASTM 2004). This test does not, however, measure the true tensile strength of the concrete. Small regions of compression are developed on the top and bottom of the specimen, leading to an overestimation of the true concrete direct tensile strength (ASTM 2004; Davies and Bose 1968). The specimen size also affects the measured tensile strength of the concrete (Shah et al. 1995; Kadlečeck et al. 2002). For instance, the splitting tensile measured in a cylindrical specimen measuring 100 × 200 mm (4 × 8 in.) would be expected to be 10% larger than that of a specimen with dimensions of 150 × 300 mm

[1]Associate Professor, Kansas State Univ., 2118 Fiedler Hall, Manhattan, KS 66506 (corresponding author). E-mail: riding@ksu.edu

[2]Senior Engineer, CTL Group, 3737 Executive Center Dr. Suite 255, Austin, TX 78731.

[3]Professor, Auburn Univ., 238 Harbert Engineering Center, Auburn, AL 36849.

[4]Associate Professor, Univ. of Texas at Austin, Civil, Architectural and Environmental Engineering Dept.-STR, 301 E. Dean Keeton St. Stop C1748, Austin, TX 78712.

[5]Professor, Univ. of Texas at Austin, Civil, Architectural and Environmental Engineering Dept.-STR, 301 E. Dean Keeton St. Stop C1748, Austin, TX 78712.

Note. This manuscript was submitted on February 7, 2013; approved on September 19, 2013; published online on September 21, 2013. Discussion period open until October 15, 2014; separate discussions must be submitted for individual papers. This paper is part of the ***Journal of Materials in Civil Engineering***, © ASCE, ISSN 0899-1561/04014058 (13)/$25.00.

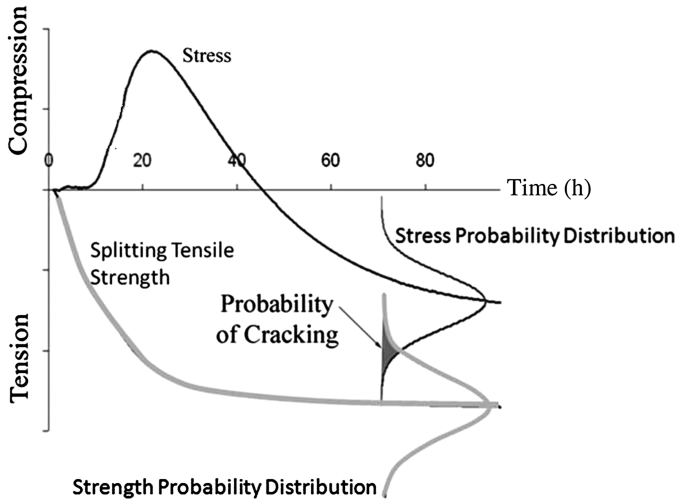

Fig. 1. Graphical representation of probability of concrete cracking (adapted from Eberhardt et al. 1994)

(6 × 12 in.) (Kadlečeck et al. 2002). Finally, the measured tensile strength of concrete is strongly influenced by the loading rate. Slower loading rates, typical of loading caused by hydration (thermal stresses), may lead to tensile strength reduction of up to 30% (Emborg 1998b). The formation of tertiary creep and microcracks in the concrete, which have additional time to propagate, may reduce the observed strength under slow loading rates (Emborg 1998b; Pijaudier-Cabot et al. 2005).

Concrete tensile strength tests are not commonly performed for construction projects. In most cases, the concrete tensile strength is estimated from its compressive strength. While there are many equations used to model the relationship between compressive strength and tensile strength at different strength ranges, many of these fit functions used to estimate the concrete tensile strength assume a power-type function based on the compressive strength as shown in Eqs. (2*a*) (psi) and (2*b*) (MPa) (Raphael 1984; Oluokun et al. 1991; Arıoglu et al. 2006; Carino and Lew 1982; ACI 2008)

$$f_{ct} = a \cdot (f_c)^b \tag{2a}$$

$$f_{ct} = \frac{a}{145.04} \cdot (f_c \cdot 145.04)^b \tag{2b}$$

where f_{ct} is the concrete splitting tensile strength (MPa or psi), a and b are fit constants, and f_c is the concrete compressive strength (MPa or psi). The fit constants a and b are the same for both English and SI units.

There are several methods to determine the stress state of concrete for input into Eq. (1). One such method for mortar is the restrained ring test. In this test method, mortar is restrained during shrinkage by a steel ring on the inside of the mortar specimen (AASHTO 2008). Another method for concrete uses a temperature stress testing machine (TSTM) (van Breugel and Lokhorst 2001), which has an active restraint system and imposes 100% restraint on the concrete. The rigid cracking frame (RCF) uses a similar concrete specimen as the TSTM but with passive restraint. The degree of restraint in the rigid cracking frame may be closer to that of a concrete column or footing, while the TSTM may simulate better the cracking in a continuously reinforced concrete pavement or some other structure subjected to 100% restraint.

The TSTM was used by van Breugel and Lokhorst (2001) to compare concrete stress at cracking to splitting tensile strength using 16 restrained concrete tests. The TSTM and RCF tests allow for the testing of concrete cracking tendency under controlled, easy-to-interpret conditions. The cracking variability seen in these tests can be used in determining the cracking probability of structures modeled analytically under similar restraint conditions. The mean cracking stress to splitting tensile strength ratio was found to be 0.75. In that study, splitting tensile strength was determined on cubes measuring 150 mm (6 in.) according to BS EN 12390-6 (Klaas van Breugel, personal communication, Dec. 14, 2011; BSI 2009). The study presented in this paper focused on establishing empirically based probability density functions of early-age concrete cracking based on measured stress from early-age restrained concrete RCF tests and the measured unrestrained concrete splitting tensile strength. Additionally, this study investigated the applicability of different fit functions available for calculating the splitting tensile strength development from the measured compressive strength for use in calculating the probability of early-age concrete cracking from thermal and autogenous deformation.

Early-age is defined in this paper as the first 4 to 5 days after concrete placement. Although the degree of restraint differs for different structures and locations in structures, thermal stress analyses commonly assume that the degree of restraint changes the stress development and not the failure criterion used. The validity of this assumption is an open question (Hossain and Weiss 2004) and could be the subject for a future study. The degree of restraint for the rigid cracking frame starts at 100% when the concrete is placed, and ultimately reaches 75 to 85%, depending on the concrete modulus development as will be discussed later. The empirical probability density functions developed in this study assume that the degree of restraint difference between concrete specimens studied changes the stress development rate and not the stress at which cracking occurs. The empirical probability density functions developed are based on one-dimensional cases of stress in the rigid cracking frame. It is unknown how the probability density functions would change for two or three dimensional states of stress. Any significant differences between field conditions and the laboratory testing conditions may cause differences in the probability density function.

Materials

Several concrete mixtures were tested as part of this study and were selected in consultation with the Texas Department of Transportation to be representative of typical mass concrete and bridge deck concrete mixtures in the United States. The base concrete mixture used in the RCF tests consisted of 335 kg/m^3 (564 lb/yd^3) of total cementitious materials and a coarse aggregate-to-total aggregate ratio of 0.6. The water-to-cementitious materials ratio (w/cm) used in the concretes ranged between 0.32 and 0.53 with a majority of the tests conducted with a w/cm of 0.42. The total amount of cementitious materials was changed to 279 kg/m^3 (470 lb/yd^3) on one test conducted at a 0.53 w/cm, 307 kg/m^3 (517 lb/yd^3) on one test conducted at a 0.48 w/cm, 362 kg/m^3 (611 lb/yd^3) on five tests conducted at a 0.38 w/cm, and 390 kg/m^3 (658 lb/yd^3) on one test conducted at a 0.32 w/cm. Seven different fly ashes [five C618 (ASTM 2003) Class F and two Class C fly ashes] were used in this study with replacement percentages varying from 20 to 40%. Two different Grade 120 slag cements were also used, with replacement levels ranging from 30 to 50%. Two ternary blends of fly ash and silica fume (25% fly ash and 6% silica fume) were tested, along with one that used both fly ash and slag cement (30%

Table 1. Cement Composition and Properties

Composition/property	IA	IB	IC	I/IIA	I/IIB	I/IIC	I/IID	I/IIE	I/IIF	I/IIG	III	V
SiO_2	19.2	20.5	21.3	20.6	20.8	21.0	20.5	20.4	20.6	21.3	20.2	21.6
Al_2O_3	5.3	5.4	5.3	4.8	3.9	4.1	4.9	4.7	5.9	5.0	5.0	4.0
Fe_2O_3	2.3	2.0	1.9	3.2	3.7	3.8	3.3	3.4	2.7	3.3	3.7	5.3
CaO	63.2	64.5	63.6	64.3	64.5	63.4	64.4	64.8	63.0	62.0	62.5	63.1
MgO	1.1	1.2	1.3	1.5	1.0	1.3	1.5	0.8	1.0	2.0	1.0	0.8
Na_2O	0.1	0.1	0.1	0.2	0.2	0.1	0.2	0.1	0.2	0.2	—	0.3
K2O	1.0	0.6	0.6	0.4	0.6	0.6	0.4	0.7	0.8	0.4	—	0.2
Na_2O_{eq}	0.8	0.5	0.5	0.4	0.6	0.5	0.5	0.6	0.7	0.5	0.3	0.4
TiO_2	0.3	0.3	0.2	0.3	0.2	0.2	0.2	0.2	0.3	0.3	—	0.2
MnO_2	0.0	0.0	0.0	0.5	0.0	0.6	0.4	0.3	0.3	0.4	—	0.1
P_2O_5	0.2	0.2	—	0.1	0.0	0.2	0.1	0.2	0.2	0.1	—	0.0
SrO	0.1	0.1	—	0.1	0.0	0.2	0.1	0.2	0.2	0.0	—	0.1
BaO	0.0	0.0	—	0.0	0.0	0.0	0.0	0.0	0.0	0.0	—	0.0
SO_3	3.2	3.4	3.6	2.8	2.4	3.0	2.8	2.7	3.1	2.6	4.6	2.7
LOI	4.1	1.8	—	1.2	2.7	1.5	1.4	1.6	1.8	2.4	1.9	1.6
Free CaO	0.0	0.0	0.0	0.0	0.0	0.0	0.6	0.0	0.0	0.5	—	0.0
ASTM C 150 Bogue compounds												
C_3S	63.1	58.3	49.0	60.4	66.5	56.5	60.7	64.9	47.5	45.2	48.8	49.9
C_2S	7.4	14.7	24.0	13.5	9.4	17.7	12.9	9.4	23.2	26.9	21.1	24.4
C_3A	10.3	11.0	10.9	7.3	4.0	4.6	7.5	6.8	11.1	7.5	7.0	1.8
C4AF	7.0	6.1	5.7	9.7	11.4	11.5	10.0	10.3	8.3	10.1	11.4	16.1
Results from Rietveld analysis												
C_3S	61.0	61.2	58.8	55.5	55.7	64.0	62.9	64.5	54.0	58.5	—	49.0
C_2S	15.6	16.0	19.2	17.4	21.1	15.3	11.0	15.3	18.6	13.8	—	26.4
C_3A	9.6	13.1	11.4	6.8	4.0	5.1	6.7	4.4	9.9	6.2	—	4.4
C_4AF	6.0	3.5	2.2	10.7	10.7	11.0	10.1	10.8	6.6	10.0	—	12.1
CSH_2 (gypsum)	5.4	5.7	6.1	4.8	4.1	5.1	4.7	4.5	5.3	4.4	—	4.7
Periclase	0.0	0.0	0.8	0.6	0.0	0.0	0.6	0.0	0.0	0.9	—	0.0
Gypsum	0.4	1.4	2.6	0.9	0.0	1.6	2.2	1.5	2.4	1.6	—	2.3
Hemihydrate	1.2	1.5	1.9	1.9	2.5	0.6	1.8	0.5	1.1	2.7	—	2.0
Anhydrite	0.7	0.6	0.8	0.9	0.7	0.6	0.6	0.6	0.5	0.5	—	0.4
K_2SO_4	1.0	1.5	2.0	0.5	0.7	0.0	0.0	0.4	1.2	1.3	—	0.9
$CaCO_3$	3.6	0.8	0.0	2.5	3.2	1.0	2.8	1.2	5.7	3.2	—	2.5
Blaine	391	350	330	405	365	349	381	354	364	330	560	409

Table 2. Supplementary Cementitious Material Composition and Properties

	Class F fly ashes					Class C fly ashes			Slag cement		Silica fume
Composition/property	FF1	FF2	FF3	FF4	FF10	FC1	FC2	FC3	S1	S2	SF
SiO_2	56.6	51.7	46.7	49.5	—	37.8	33.1	37.4	34.5	34.0	94.3
Al_2O_3	30.7	24.8	19.7	17.6	—	19.8	18.4	17.7	11.4	11.4	0.0
Fe_2O_3	4.9	4.2	5.1	5.5	—	6.2	5.4	5.9	0.7	1.2	0.1
CaO	0.7	13.1	18.4	19.5	—	23.1	28.9	25.9	41.7	41.7	0.5
MgO	0.7	2.3	3.0	2.8	—	4.6	5.3	5.2	7.3	8.3	0.6
Na_2O	0.1	0.2	1.8	0.6	—	1.7	1.6	1.6	0.1	0.2	0.1
K_2O	2.3	0.8	0.9	1.0	—	0.1	0.4	0.6	0.4	0.3	1.0
$Na_2O + 0.658 * K_2O$	1.6	0.7	2.3	1.2	—	1.8	1.9	2.0	0.4	0.4	0.7
SO_3	0.0	0.5	0.8	1.1	—	1.5	2.3	1.8	1.9	1.2	0.2
LOI	2.1	0.2	0.4	0.4	—	0.7	0.3	0.5	0.8	0.8	3.1
Blaine	147	166	420	296	—	348	300	588	332	320	20000

fly ash and 30% slag cement). Five C150 (ASTM 2011) Type I cements, three Type I/II cements, one Type III cement, and one Type V cement were used in the testing. Siliceous river gravel, limestone, and dolomitic limestone coarse aggregate were used in the concrete. Dolomitic limestone sand was used in one mixture, while natural river sand was used in all other tests. Cement and SCM composition and properties, and mixture proportions for the mixtures used in the rigid cracking frame tests and other splitting tensile and compressive strength testing are given in Tables 1–14.

Experimental Methods

Rigid Cracking Frame Experiments

The stress level at cracking due to thermal and autogenous shrinkage was investigated using a RCF (Mangold 1998). The rigid cracking frame uses a passive restraint system, as shown in Fig. 2 during concrete placement. When the concrete temperature changes and the concrete experiences autogenous shrinkage, the concrete deformations are restrained by the two large Invar steel bars. Before the

Table 3. Concrete Mixtures Made with Cement IA

SCM 1	SCM 1%	SCM 2	SCM 2%	Cement + SCM kg/m^3 (lb/yd^3)	w/cm	CA type	FA/(FA + CA)	Chemical admixtures used	Mixture used in cracking frame?
FF1	20	—	—	335 (564)	0.44	SRG	0.44	—	N
FF1	30	—	—	335 (564)	0.44	SRG	0.44	—	N
FF1	30	—	—	335 (564)	0.44	SRG	0.44	—	N
FF1	40	—	—	335 (564)	0.44	SRG	0.44	—	N
FF1	20	SF	5	335 (564)	0.44	SRG	0.44	HRWR-N	N
FF4	20	—	—	314 (529)	0.4	L	0.45	LRWRR, AEA	N
FC2	40	—	—	335 (564)	0.44	SRG	0.45	—	N
FC2	20	—	—	335 (564)	0.44	SRG	0.45	—	N
FC2	30	—	—	335 (564)	0.44	SRG	0.45	—	N
FC2	30	SF	5	335 (564)	0.44	SRG	0.44	—	N
FC2	35	SF	5	335 (564)	0.44	SRG	0.44	—	N
FC2	30	—	—	335 (564)	0.38	SRG	0.45	—	N
FC2	30	—	—	335 (564)	0.38	SRG	0.45	HRWR-N	N
FC2	30	SF	8	335 (564)	0.32	SRG	0.44	HRWR-PC	N
FC2	30	UFFA	8	335 (564)	0.32	SRG	0.44	HRWR-PC	N
FC2	30	UFFA	12	335 (564)	0.32	SRG	0.44	HRWR-PC	N
FC2	30	SF	5	335 (564)	0.32	SRG	0.44	HRWR-PC	N
FC1	20	—	—	335 (564)	0.44	SRG	0.45	—	N
FC1	30	—	—	335 (564)	0.44	SRG	0.45	—	N
FC1	40	—	—	335 (564)	0.44	SRG	0.44	—	N
FC1	30	—	—	335 (564)	0.44	SRG	0.45	ACC	N
FC1	30	—	—	368 (620)	0.4	SRG	0.46	RET	N
FC3	30	SF	8	335 (564)	0.32	Jobe	0.44	HRWR-N	N
FC3	30	UFFA	7.5	335 (564)	0.32	Jobe	0.44	HRWR-N, RET	N
FF2	20	—	—	319 (538)	0.68	SRG	0.40	HRWR-N	N
FF2	30	—	—	332 (560)	0.6	SRG	0.40	LRWR	N
FF2	20	—	—	335 (564)	0.53	SRG	0.40	—	N
FF2	30	—	—	335 (564)	0.45	SRG	0.42	—	N
FF2	40	—	—	335 (564)	0.44	SRG	0.44	—	N
FF2	20	—	—	335 (564)	0.44	SRG	0.44	—	N
FF2	20	—	—	335 (564)	0.44	SRG	0.44	ACC	N
FF2	20	—	—	319 (538)	0.44	SRG	0.44	AEA	N
S1	30	—	—	335 (564)	0.44	SRG	0.45	—	N
S1	40	—	—	335 (564)	0.44	SRG	0.45	—	N
S1	50	—	—	335 (564)	0.44	SRG	0.45	—	N
S1	50	—	—	335 (564)	0.44	SRG	0.45	ACC	N
S1	50	—	—	335 (564)	0.44	SRG	0.45	RET	N
S1	70	—	—	335 (564)	0.44	SRG	0.45	—	N
SF	5	—	—	335 (564)	0.44	SRG	0.45	—	N
—	—	—	—	335 (564)	0.44	SRG	0.45	—	N
—	—	—	—	335 (564)	0.44	SRG	0.45	—	N
—	—	—	—	335 (564)	0.44	SRG	0.45	—	N
—	—	—	—	335 (564)	0.44	SRG	0.45	ACC	N
—	—	—	—	335 (564)	0.44	SRG	0.45	ACC	N
—	—	—	—	335 (564)	0.44	SRG	0.45	RET	N
—	—	—	—	335 (564)	0.4	SRG	0.46	RET	N
—	—	—	—	335 (564)	0.4	SRG	0.46	RET	N
—	—	—	—	335 (564)	0.44	SRG	0.45	ACC	N
—	—	—	—	335 (564)	0.38	SRG	0.45	HRWR-PC	N
—	—	—	—	335 (564)	0.44	SRG	0.45	HRWR—PC	N
—	—	—	—	335 (564)	0.38	SRG	0.45	HRWR_PC, CI	N
—	—	—	—	317 (534)	0.44	SRG	0.45	HRWR—N	N

Note: ACC = ASTM C 494 type C accelerator; AEA = air entraining admixture; CI = calcium nitrite corrosion inhibitor; LRWRR = ASTM C 494 type B & D water reducing and retarding admixture; RET = ASTM C 494 Type B retarder; MRWR = midrange water reducer; HRWR-N = ASTM C 494 Type F naphthalene, sulfonate-based, high-range, water-reducing admixture; HRWR-PC = ASTM C 494 type F polycarboxylate-based, high-range, water-reducing admixture.

concrete sets, the concrete elastic modulus is essentially zero, meaning that stresses do not develop until after setting and the elastic modulus increases. When hydration causes the concrete temperature to increase, the concrete expansion is converted into compressive stresses as shown in Fig. 3. At the same time that a compressive stress develops in the rigid cracking frame concrete, tensile stresses develop in the Invar sidebars to maintain equilibrium. The concrete compressive stress is simultaneously reduced by stress relaxation and the eventual concrete temperature decrease. As the concrete temperature continues to decrease, tensile stresses develop in the concrete and the stress state in the Invar sidebars becomes compressive. For the same magnitude of temperature change, the increased elastic modulus from continued hydration results in higher stresses on cooling than what the concrete

Table 4. Concrete Mixtures Made with Cement IB

SCM 1	SCM 1%	SCM 2	SCM 2%	Cement + SCM kg/m^3 (lb/yd^3)	w/cm	CA type	FA/(FA + CA)	Chemical admixtures used	Mixture used in cracking frame?
—	—	—	—	335 (564)	0.42	SRG	0.40	LRWRR	Y
—	—	—	—	335 (564)	0.42	SRG	0.40	LRWRR	Y
—	—	—	—	335 (564)	0.42	SRG	0.40	LRWRR	Y
—	—	—	—	335 (564)	0.42	SRG	0.40	LRWRR	Y
—	—	—	—	335 (564)	0.42	SRG	0.40	LRWRR	Y
—	—	—	—	390 (657)	0.32	SRG	0.40	LRWRR, HRWR—PC	Y
—	—	—	—	307 (517)	0.48	SRG	0.40	—	Y
—	—	—	—	279 (470)	0.53	SRG	0.40	—	Y
FC1	30	—	—	335 (564)	0.42	SRG	0.40	LRWRR	Y
FC1	30	—	—	335 (564)	0.42	SRG	0.40	LRWRR	N
FC1	30	—	—	335 (564)	0.42	SRG	0.40	LRWRR	Y
FC1	30	—	—	335 (564)	0.42	SRG	0.40	LRWRR	Y
FF2	30	—	—	335 (564)	0.42	SRG	0.40	LRWRR	Y
FF2	30	—	—	335 (564)	0.42	SRG	0.40	LRWRR	Y
FF2	30	—	—	335 (564)	0.42	SRG	0.40	LRWRR	Y
FF2	30	—	—	335 (564)	0.42	SRG	0.40	LRWRR	N
FF2	30	—	—	335 (564)	0.42	SRG	0.40	LRWRR	N
S1	50	—	—	335 (564)	0.42	SRG	0.40	LRWRR	Y
S1	50	—	—	335 (564)	0.42	SRG	0.40	LRWRR	Y
S1	30	—	—	335 (564)	0.42	SRG	0.40	LRWRR	Y
S1	30	—	—	335 (564)	0.42	SRG	0.40	LRWRR	Y
—	—	—	—	363 (612)	0.38	SRG	0.40	LRWRR, HRWR—PC	Y
—	—	—	—	335 (564)	0.42	SRG	0.40	LRWRR	Y
—	—	—	—	335 (564)	0.42	SRG	0.40	LRWRR	Y
—	—	—	—	335 (564)	0.42	SRG	0.40	LRWRR	Y
—	—	—	—	335 (564)	0.42	SRG	0.40	LRWRR	Y
—	—	—	—	335 (564)	0.42	SRG	0.40	LRWRR	Y
—	—	—	—	335 (564)	0.32	SRG	0.40	HRWR-PC	Y
—	—	—	—	335 (564)	0.42	L	0.40	HRWR-PC	N
—	—	—	—	335 (564)	0.42	L	0.40	HRWR-PC	Y
—	—	—	—	335 (564)	0.42	L	0.40	HRWR-PC	N

experienced when heating. For example, a concrete mixture at 8 h of age with a modulus of 6,895 MPa (1,000,000 psi) and coefficient of thermal expansion (CTE) of 10×10^{-6} m/m/°C (5.6×10^{-6} in./in./°F) and increase in temperature of 10°C (18°F) would result in a compressive stress increase of 0.69 MPa (101 psi). That same concrete mixture at 16 h with a modulus of 20.7 GPa (3,000,000 psi) and the same CTE and a temperature decrease of 10°C (18°F) would result in a tensile stress increase of 2.07 MPa (302 psi). Eventually, when the tensile stress exceeds the tensile strength of the specimen, it cracks.

The concrete stresses may be obtained by strain gauges that are mounted on the Invar steel bars because the rigid cracking frame is a statically determinant structure. The restraint provided by the cracking frame is 100% at the time of placement (because the

Table 5. Concrete Mixtures Made with Cement IC

SCM 1	SCM 1%	SCM 2	SCM 2%	Cement + SCM kg/m^3 (lb/yd^3)	w/cm	CA type	FA/(FA + CA)	Chemical admixtures used	Mixture used in cracking frame?
—	—	—	—	363 (612)	0.38	SRG	0.40	LRWRR, HRWR-PC	Y
—	—	—	—	363 (612)	0.38	SRG	0.40	LRWRR, HRWR-PC	Y
—	—	—	—	363 (612)	0.38	SRG	0.40	LRWRR, HRWR-PC	Y
—	—	—	—	363 (612)	0.38	SRG	0.40	LRWRR, HRWR-PC	Y
—	—	—	—	335 (564)	0.42	SRG	0.40	AEA	Y
FC1	25	SF	6	335 (564)	0.42	SRG	0.39	LRWRR	Y
FC2	30	—	—	335 (564)	0.42	SRG	0.40	LRWRR	Y
FC2	20	—	—	335 (564)	0.42	SRG	0.40	LRWRR	Y
FF2	25	SF	6	335 (564)	0.42	SRG	0.39	LRWRR	Y
FF2	30	S1	30	335 (564)	0.42	SRG	0.40	LRWRR	Y
S1	50	—	—	335 (564)	0.42	SRG	0.40	LRWRR	Y
S1	50	—	—	335 (564)	0.42	SRG	0.40	LRWRR	Y
S1	50	—	—	335 (564)	0.42	SRG	0.40	LRWRR	Y
Sl	30	—	—	335 (564)	0.42	SRG	0.40	LRWRR	Y
Sl	30	—	—	335 (564)	0.42	SRG	0.40	LRWRR	Y
Sl	30	—	—	335 (564)	0.42	SRG	0.40	LRWRR	Y
Sl	30	—	—	335 (564)	0.42	SRG	0.40	LRWRR	Y
—	—	—	—	333 (564)	0.42	L	0.40	HRWR-PC	Y

Table 6. Concrete Mixtures Made with Cement I/IIA

SCM 1	SCM 1%	SCM 2	SCM 2%	Cement + SCM kg/m^3 (lb/yd^3)	w/cm	CA type	FA/(FA + CA)	Chemical admixtures used	Mixture used in cracking frame?
FF4	20	—	—	314 (529)	0.42	L	0.45	LRWRR, AEA	N
FF4	20	—	—	315 (531)	0.42	L	0.45	LRWRR, AEA	N
FF4	20	—	—	314 (529)	0.4	L	0.45	LRWRR, AEA	N
FF4	26.2	—	—	329 (554)	0.47	L	0.44	LRWRR	N
FF4	26.4	—	—	405 (683)	0.41	L	0.40	LRWRR	N
—	—	—	—	335 (564)	0.44	L	0.45	—	N

Table 7. Concrete Mixtures Made with Cement I/IIB

SCM 1	SCM 1%	SCM 2	SCM 2%	Cement + SCM kg/m^3 (lb/yd^3)	w/cm	CA Type	FA/(FA + CA)	Chemical admixtures used	Mixture used in cracking frame?
FF1	30	—	—	335 (564)	0.44	SRG	0.44	—	N
FF1	40	—	—	335 (564)	0.44	SRG	0.45	—	N
FF1	20	—	—	335 (564)	0.44	SRG	0.44	—	N
FC2	20	—	—	335 (564)	0.44	SRG	0.45	—	N
FC2	30	—	—	335 (564)	0.44	SRG	0.44	—	N
FC2	40	—	—	335 (564)	0.44	SRG	0.44	—	N
FC2	30	SF	5	335 (564)	0.44	SRG	0.45	—	N
FC1	20	—	—	335 (564)	0.44	SRG	0.45	—	N
FC1	30	—	—	335 (564)	0.44	SRG	0.45	—	N
FC1	40	—	—	335 (564)	0.44	SRG	0.44	—	N
FF2	30	—	—	335 (564)	0.44	SRG	0.45	—	N
FF2	20	—	—	335 (564)	0.44	SRG	0.44	—	N
FF2	40	—	—	335 (564)	0.44	SRG	0.45	—	N
FF2	30	—	—	335 (564)	0.44	SRG	0.45	—	N
S1	50	—	—	335 (564)	0.44	SRG	0.45	—	N
S1	50	—	—	335 (564)	0.44	SRG	0.45	ACC	N
UFFA	15	—	—	335 (564)	0.44	SRG	0.45	—	N
—	—	—	—	325 (564)	0.53	SRG	0.45	—	N
—	—	—	—	335 (564)	0.44	SRG	0.45	—	N
—	—	—	—	338 (570)	0.48	SRG	0.44	—	N
—	—	—	—	337 (568)	0.53	SRG	0.45	—	N
—	—	—	—	335 (564)	0.44	SRG	0.45	RET	N
—	—	—	—	335 (564)	0.44	SRG	0.45	RET	N
—	—	—	—	335 (564)	0.44	SRG	0.45	HRWR-N	N
—	—	—	—	335 (564)	0.42	SRG	0.40	LRWRR	Y
—	—	—	—	335 (564)	0.42	SRG	0.40	LRWRR	Y
—	—	—	—	335 (564)	0.42	SRG	0.40	LRWRR	Y
—	—	—	—	335 (564)	0.42	SRG	0.40	LRWRR	Y

Table 8. Concrete Mixtures Made with Cement I/IIC

SCM 1	SCM 1%	SCM 2	SCM 2%	Cement + SCM kg/m^3 (lb/yd^3)	w/cm	CA Type	FA/(FA + CA)	Chemical admixtures used	Mixture used in cracking frame?
FF1	30	—	—	335 (564)	0.44	SRG	0.44	—	N
FC2	30	—	—	335 (564)	0.44	SRG	0.45	—	N
FC2	30	—	—	387 (652)	0.38	SRG	0.45	HRWR-N	N
FC1	30	—	—	335 (564)	0.44	SRG	0.45	—	N
FF2	30	—	—	335 (564)	0.44	SRG	0.45	—	N
S2	48	—	—	348 (587)	0.44	SRG	0.43	HRWR-N, AEA	N
—	—	—	—	335 (564)	0.44	SRG	0.45	—	N
—	—	—	—	335 (564)	0.44	SRG	0.45	RET	N
—	—	—	—	335 (564)	0.44	SRG	0.45	ACC	N
—	—	—	—	335 (564)	0.44	SRG	0.45	HRWR-N	N
—	—	—	—	335 (564)	0.44	SRG	0.45	HRWR-PC	N
—	—	—	—	335 (564)	0.44	SRG	0.45	LRWRR	N

stiffness of the Invar steel bars is infinitely greater than that of freshly placed plastic concrete) and can decrease as the concrete modulus increases to 75 to 80%, depending on the concrete elastic modulus. The degree of restraint provided can be determined as shown in Eq. (3) (Mangold 1998)

$$\delta = \frac{100}{1 + \left(\frac{E_c A_c}{E_s A_s}\right)} \tag{3}$$

where δ is the degree of restraint (%), E_c is the concrete elastic modulus (MPa), A_c is the concrete cross-sectional area (m^2),

Table 9. Concrete Mixtures Made with Cement I/IID

SCM 1	SCM 1%	SCM 2	SCM 2%	Cement + SCM kg/m^3 (lb/yd^3)	w/cm	CA Type	FA/(FA + CA)	Chemical admixtures used	Mixture used in cracking frame?
FF3	28.6	—	—	351 (592)	0.35	SRG	0.38	LRWRR, MRWR	N
FF3	28.6	—	—	351 (592)	0.35	SRG	0.38	LRWRR, MRWR	N
FF3	40	—	—	335 (564)	0.44	SRG	0.45	—	N
FF3	30.9	—	—	362 (610)	0.35	SRG	0.38	LRWRR, MRWR	N
FF3	30.9	—	—	362 (610)	0.35	SRG	0.38	LRWRR, MRWR	Y

Table 10. Concrete Mixtures Made with Cement I/IIE

SCM 1	SCM 1%	SCM 2	SCM 2%	Cement + SCM kg/m^3 (lb/yd^3)	w/cm	CA Type	FA/(FA + CA)	Chemical admixtures used	Mixture used in cracking frame?
FF4	40	—	—	297 (501)	0.35	SRG	0.42	LRWRR, HRWR—N	N
FC1	40	—	—	335 (564)	0.44	SRG	0.44	—	N
S1	30	—	—	335 (564)	0.44	SRG	0.45	—	N
S1	40	—	—	335 (564)	0.44	SRG	0.45	—	N
S1	50	—	—	335 (564)	0.44	SRG	0.45	—	N
—	—	—	—	297 (501)	0.35	SRG	0.42	LRWRR, HRWR—N	Y

Table 11. Concrete Mixtures Made with Cement I/IIF

SCM 1	SCM 1%	SCM 2	SCM 2%	Cement + SCM kg/m^3 (lb/yd^3)	w/cm	CA Type	FA/(FA + CA)	Chemical admixtures used	Mixture used in cracking frame?
FC3	20	—	—	316 (533)	0.4	Granite	0.40	LRWRR, AEA	N
FC3	19	—	—	316 (533)	0.4	SRG	0.40	LRWRR, AEA	N
—	—	—	—	261 (440)	0.48	SRG	0.40	LRWRR, AEA	N
—	—	—	—	335 (564)	0.44	SRG	0.40	—	N

Table 12. Concrete Mixtures Made with Cement I/IIG

SCM 1	SCM 1%	SCM 2	SCM 2%	Cement + SCM kg/m^3 (lb/yd^3)	w/cm	CA Type	FA/(FA + CA)	Chemical admixtures used	Mixture used in cracking frame?
FF10	25	—	—	347 (585)	0.45	dolomite	0.40	LRWRR, AEA	N
FF10	25	—	—	347 (585)	0.45	dolomite	0.40	LRWRR, AEA	Y
FF10	25	—	—	347 (585)	0.45	SRG	0.40	LRWRR, AEA	Y
FF10	25	—	—	347 (585)	0.45	dolomite	0.40	LRWRR, AEA	Y
FF10	25	—	—	347 (585)	0.45	dolomite	0.40	LRWRR, AEA	N

Table 13. Concrete Mixtures Made with Cement III

SCM 1	SCM 1%	SCM 2	SCM 2%	Cement + SCM kg/m^3 (lb/yd^3)	w/cm	CA Type	FA/(FA + CA)	Chemical admixtures used	Mixture used in cracking frame?
—	—	—	—	335 (564)	0.42	SRG	0.40	LRWRR	Y
—	—	—	—	335 (564)	0.42	SRG	0.40	LRWRR	Y
—	—	—	—	335 (564)	0.42	SRG	0.40	LRWRR	Y
—	—	—	—	335 (564)	0.42	SRG	0.40	LRWRR	Y
—	—	—	—	335 (564)	0.42	SRG	0.40	LRWRR	Y

E_s is the Invar sidebar modulus (MPa), and A_s is the Invar sidebar's cross sectional area (m^2). The Invar bar stiffness determined by the Invar modulus and area were found through calibration of the frame by loading the frame with a hydraulic ram with a calibrated load cell between the ram and frame. The formwork was slightly shorter than the distance between the frame crossheads, with the gap sealed by silicone. Invar steel is used because of the material's low coefficient of thermal expansion, which reduces the measurement errors caused by the thermal movement of the sidebars. The thermal movement of the Invar sidebars can be calculated as

$$\varepsilon_{Tadj} = \Delta T_{ib} \cdot \alpha_{ib} \cdot \delta \quad (4)$$

where ε_{Tadj} is the temperature-induced strain of the Invar bar, ΔT_{ib} is the temperature change of the Invar sidebar at the strain gauge (in degrees Celsius), and α_{ib} is the coefficient of thermal expansion of

Table 14. Concrete Mixtures Made with Cement V

SCM 1	SCM 1%	SCM 2	SCM 2%	Cement + SCM kg/m^3 (lb/yd^3)	w/cm	CA Type	FA/(FA + CA)	Chemical admixtures used	Mixture used in cracking frame?
FF1	30	—	—	335 (564)	0.44	SRG	0.44	—	N
FC2	30	—	—	335 (564)	0.44	SRG	0.44	—	N
FF2	30	—	—	335 (564)	0.44	SRG	0.44	—	N
S1	40	—	—	335 (564)	0.44	SRG	0.45	HRWR-N	N
S1	40	—	—	335 (564)	0.44	SRG	0.45	—	N
—	—	—	—	335 (564)	0.44	SRG	0.44	—	N
—	—	—	—	332 (560)	0.44	SRG	0.45	MRWR	Y
—	—	—	—	332 (560)	0.44	SRG	0.45	MRWR	Y
—	—	—	—	332 (560)	0.44	SRG	0.45	MRWR	Y
—	—	—	—	335 (564)	0.44	SRG	0.40	MRWR	Y
—	—	—	—	335 (564)	0.44	SRG	0.40	MRWR	Y
—	—	—	—	335 (564)	0.44	SRG	0.40	HRWR-PC	Y

Fig. 2. Rigid cracking frame

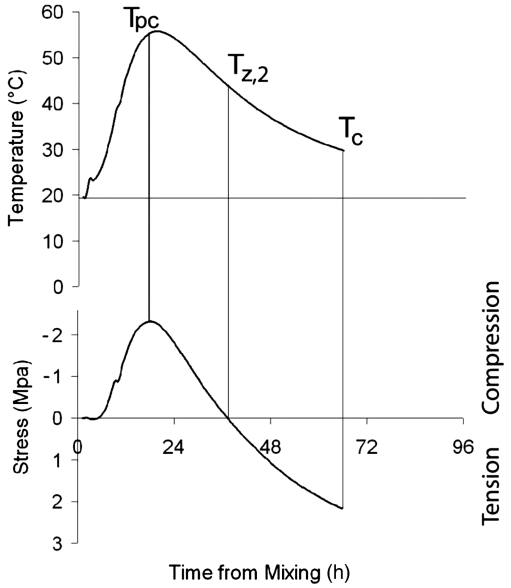

Fig. 3. Rigid cracking frame temperature development and corresponding early-age concrete stress development; $\mathbf{T}_{pc}$ is the concrete temperature at the peak compressive stress in the concrete, $\mathbf{T}_{z,2}$ is the concrete temperature at the time of the second zero stress point, and $\mathbf{T}_c$ is the concrete temperature at cracking (1 MPa = 145 psi, 1°C = 1.8°F) (adapted from Springenschmid and Breitenbücher 1998)

the Invar bar, which is 1×10^{-6} m/m/°C (0.6×10^{-6} in./in./°F) for the frame used in this study. These corrections were typically small and between 3 and 7% of the cracking stress. For a correction of 5% of the cracking stress, even a 20% error in the correction would amount to only 1% of the cracking stress. Steel cross bars with friction connections were used on the top and bottom of the frame to prevent any slipping of the specimen in the grips. The RCF (RILEM Technical Committee 119-TCE 1998) samples tested in this study had a cross section of 150 × 150 mm (6 × 6 in.).

In some tests, microcracking occurred before a final through-crack, as shown in Fig. 4. This usually occurred when high-strength concrete was used and has been reported by other researchers (Schrage and Summer 1994). The cracking stress used for calculating stress-to-strength ratios at the time of cracking was the first significant crack measured during the test, whether it was a microcrack or a through-crack.

Concrete Temperature Profiles

The temperature in the sealed concrete was controlled by circulating temperature-controlled water through copper pipes embedded in the RCF formwork. In all tests, if the concrete did not crack within 96 hours after mixing, the concrete was cooled at 1°C/h

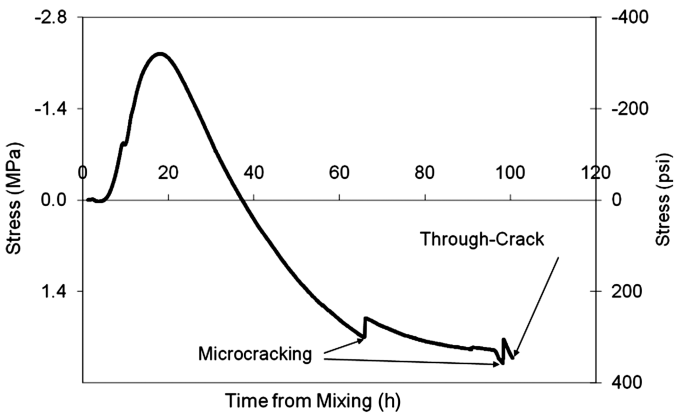

Fig. 4. Types of cracking observed in rigid cracking frame specimens

Table 15. Description of Rigid Cracking Frame Specimen Temperature Conditions

Type of structure modeled	Location in concrete member of predicted temperature used	Temperature condition imposed on concrete member surface in model	Number of RCF specimens
1 m (39.4 in.)-thick wall	Wall center in one-dimensional heat transfer model	Constant enforced surface temperature	59
0.75 m (29.6 in.)-thick wall	Wall center in one-dimensional heat transfer model	Constant enforced surface temperature	1
200 mm (8 in.)-thick bridge deck	100 mm (4 in.) from simulated bridge deck top surface using one-dimensional heat transfer model	Realistic heat transfer with environment as described in (Riding et al. 2009)	2
200 mm (8 in.)-thick bridge deck	Measured concrete temperature at midheight of a 200 mm (8 in.) actual bridge deck (Riding et al. 2009)	Actual concrete temperature used	1
No active temperature control—concrete heat of hydration and form insulation drove temperature change			1

(1.8°F/h) until cracking occurred. A total of 64 RCF tests were conducted for the work presented in this paper. Of these 64 tests, the temperature profile was enforced on 60 RCF tests to be that calculated for the temperature at the center of a hypothetical walls 0.75 m (29.5 in.) and 1 m (39.4 in.) thick with a constant surface temperature simulated using finite difference model and the heat generated calculated from semiadiabatic calorimetry. In another RCF test, the concrete was allowed to cure with no active temperature control. In this test, the temperature change occurred because of the concrete heat of hydration and heat loss through the form insulation. The tests using no active temperature control and a hypothetical wall 0.75 m (29.5 in.) thick were conducted in order to investigate the effects of temperature development on stress development in order to establish a common testing protocol between two laboratories. The RCF tests using the temperature predicted for a wall 1 m (39.4 in.) thick were conducted to investigate the effects of temperatures more commonly found in mass concrete on stress development and stress relaxation. The temperature profile for two RCF tests was enforced to be that calculated at midheight of a simulated bridge deck 200 mm (8 in.) thick. An additional RCF test was performed using the measured temperature profile at midheight of an actual bridge deck 200 mm (8 in.) thick placed in Austin, TX, at 10 a.m. on August 17, 2006, as described by (Riding et al. 2009). The three tests performed using temperature profiles from bridge decks were conducted in order to investigate the effects of placement time on bridge deck stresses as part of a separate project than those conducted for mass concrete. Table 15 provides a summary of the RCF concrete temperature profiles used.

The stress development plots of a few representative RCF tests are presented to illustrate the various temperature and stress profiles measured in the RCF. Fig. 5 shows the temperature history and corresponding measured stress development in the rigid cracking frame from the RCF test performed using the actual temperature at middepth of a bridge deck 200 mm (8 in.) thick (Riding et al. 2009). The test shown in Fig. 5 used materials collected from the ready-mixed concrete batch plant used for the bridge deck. Fig. 6 shows the results from another RCF test where the concrete was allowed to cure with no active temperature control. Any temperature rise in this test occurred because the formwork was insulated during curing. The concrete mixture in this test used 332 kg/m^3 (560 lb/yd^3) of Type V cement at a 0.44 w/cm, and a midrange water reducer with 1,076 kg/m^3 (1813 lb/yd^3) of siliceous river gravel and 872 kg/m^3 (1469 lb/yd^3) of a natural siliceous sand. Also in Fig. 6 are the temperature development and corresponding stress development for two tests measured in the rigid cracking frame with the temperature adjusted to that of simulated wall thickness of 0.75 m (29.5 in.) and 1 m (39.4 in.) with identical concrete mixture proportions as used in the test cured with no active temperature control.

Concrete Mechanical Properties

Twenty-four 100 × 200 mm (4 × 8 in.) concrete cylinders were match cured to the concrete temperatures measured in the middle of the cracking frame for each RCF test performed. The temperature in the middle of the cracking frame specimens was measured using a type T thermocouple. Two compression and two splitting tensile tests were performed on the cylinders at approximately 0.5, 1, 2, 3, 7, and 28 calendar days to monitor the strength development of the concrete. The RCF specimen cracking times did not coincide with the times for measuring the splitting tensile strength. The splitting tensile strength at the time of cracking was determined by first fitting Eq. (5) to the measured compressive strength

$$f_c = f_{\text{cult}} e^{-(\tau_s/t_e)^{\beta_s}} \tag{5}$$

where f_c is the compressive strength (MPa), t_e is the concrete equivalent age calculated according to C1074 (ASTM 2010), and f_{cult} (MPa), τ_s (h), and β_s are fit constants. Activation energies used to calculate the concrete equivalent age were taken from the literature (Brooks et al. 2007). Activation energy values of 40,700 J/mol for mixtures containing no SCMs, 45,000 J/mol

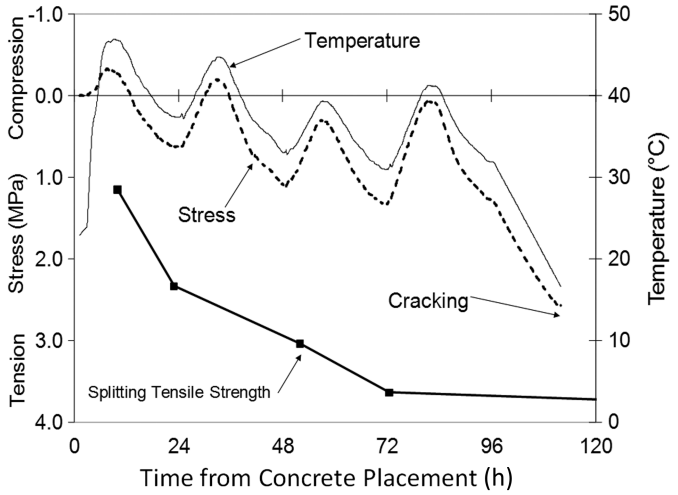

Fig. 5. Temperature and stress development enforced on a rigid cracking frame test simulating the measured bridge deck temperature profile with the splitting tensile strength (1 MPa = 145 psi, 1°C = 1.8°F) (adapted from Riding et al. 2009)

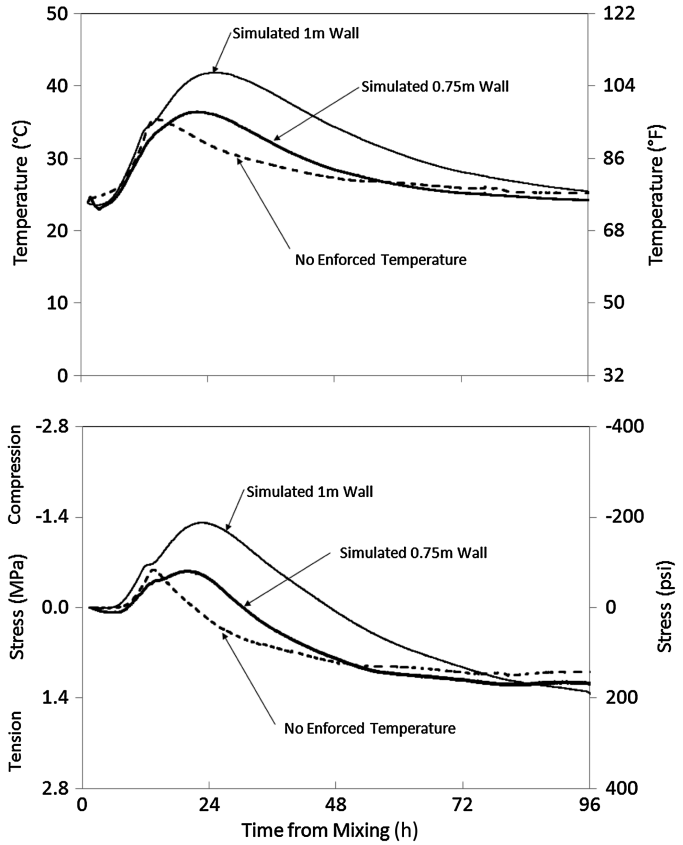

Fig. 6. Temperature development for the same concrete mixture proportions under three temperature scenarios: no enforced temperature, simulated wall 0.75 m (29.5 in.) thick, and simulated wall 1 m (39.4 in.) thick; the concrete mixture used in all of these RCF tests used a Type V cement, siliceous river gravel, and a natural siliceous river sand

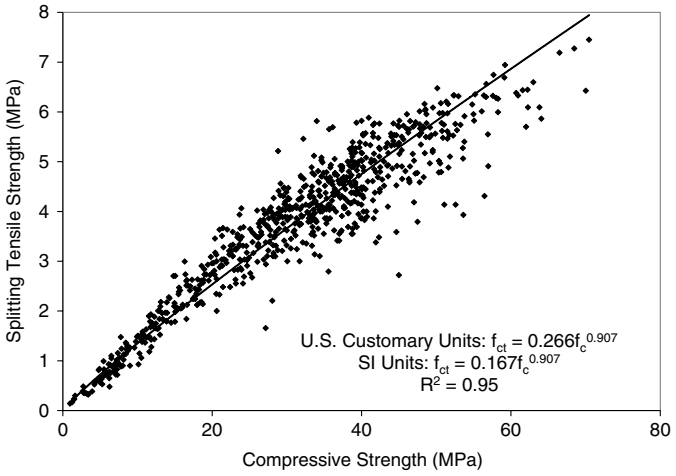

Fig. 7. Relationship between measured compressive strength and splitting tensile strength (1 MPa = 145 psi)

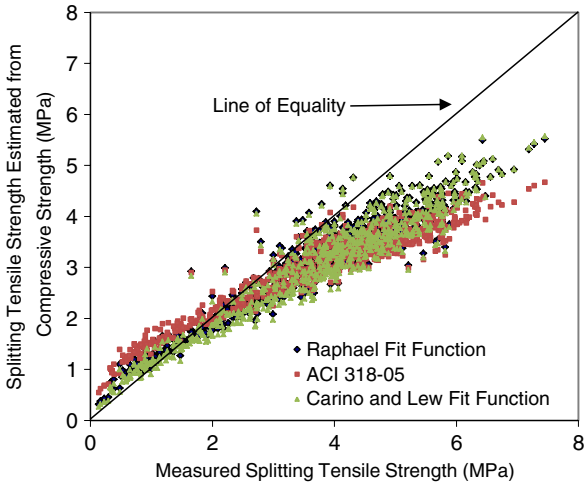

Fig. 8. Comparison of measured splitting tensile strength values and calculated values using $a = 1.7$ and $b = 2/3$ (1 MPa = 145 psi)

for mixtures containing Class F fly ash, 44000 J/mol for mixtures containing Class C fly ash, and 41,000 J/mol for mixtures containing slag cement were chosen. Any errors in the activation energy used should have little impact on the results because the concrete cylinders used to measure the strength were match cured to the cracking frame specimens.

In addition to the cylinders made from the same batches of concrete as the RCF specimens that were match cured to the RCF specimens, 405 compression and splitting tensile tests were performed on additional concrete mixtures cast and cured at room temperature and 100% relative humidity and tested at 1, 7, 28, and 91 days. These tests were used to further examine the relationship between compressive strength and splitting tensile strength development. These mixtures can be identified in Tables 3–14 that describe the concrete mixtures tested as mixtures that were not used in the cracking frame for determining the stress-to-splitting tensile strength ratio, and were only used to compare the relationship between compressive and splitting tensile strength.

Results

Fit Functions for Calculating the Splitting Tensile Strength Development from the Measured Compressive Strength

A total of 743 compressive and splitting tensile strength tests were used to determine the relationship between the two parameters. The power-law equation described in Eq. (2) correctly modeled the relationship between the measured splitting tensile strength and the compressive strength as shown in Fig. 7. Fit constants a and b were found to be 0.266 and 0.907, respectively, with the coefficient of determination (r^2) equal to 0.95. For a fixed a-value, any formulation with a power lower than 0.907 overestimates the splitting tensile strength of the concrete at lower compressive strengths and underestimates the splitting tensile strength at the higher compressive strengths. This is shown in Fig. 8 using a fit equation of $a = 1.7$ and $b = 2/3$ as suggested by Raphael (1984) and referred to in this paper as the Raphael fit function. Fig. 8 also shows the relationship between calculated and measured splitting tensile strength for the ACI 318 equation and the Carino and Lew (1982) fit function.

Measured Concrete Stress-to-Strength Ratio

The stress-to-strength ratio of the RCF tests was determined by dividing the measured RCF stress at the first crack to the splitting tensile strength fit using Eqs. (2) and (5) to splitting tensile strength tests on cylinders match cured to the RCF temperature. Ratios of the measured concrete stress at cracking to the measured splitting

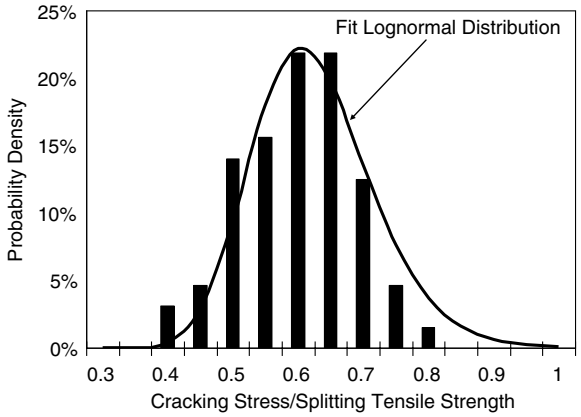

Fig. 9. Measured cracking stress to splitting tensile strength ratio distribution

tensile strength ranged between 0.37 and 0.79. The distribution was fit well by a lognormal-type distribution, as shown in Fig. 9, with a 50% probability of cracking occurring at a stress-to-strength ratio of 0.57 and a standard deviation of 0.16. The lognormal distribution also met the constraint that the stress-to-strength ratio cannot be negative (Johnson 2000).

Stress-to-Strength Ratio Probability Density Functions Using Splitting Tensile Strength Fit Functions

The measured concrete stress at cracking was compared to the estimated concrete splitting tensile strength from the measured compressive strength. The splitting tensile strengths were estimated using several different fit functions [all based on Eq. (2)] that have been developed to predict the concrete splitting tensile strength from the compressive strength. The first fit function used for predicting the splitting tensile strength was based on the splitting tensile and compressive strength tests performed in this study, hereafter called the proposed fit function. The second fit function examined was the Raphael fit function (Raphael 1984). A third fit function used was that suggested in the ACI 318 building code (ACI 2008) for calculating the splitting tensile strength from compressive strength tests with $a = 6.7$ and $b = 0.5$, hereafter referred to as the ACI 318-08 fit function. Finally, a fit function developed by Carino and Lew (1982) was examined in this study.

The fit constants for each fit function according to Eq. (2) and the maximum and minimum measured stress-to-estimated strength ratios at cracking for the 64 tests are summarized in Table 16. The first column in Table 16 gives the information on the lognormal fit to the measured stress-to-measured splitting tensile strength ratios at cracking, whereas the remainder of the columns present the measured stress-to-splitting tensile strength estimated from the concrete compressive strength. Table 16 also shows the mean and standard deviation of a lognormal distribution of the probability of cracking fit to the stress-to-strength ratio at cracking, as well as three commonly used tests for gauging the goodness of fit of the lognormal distribution to the data. The Kolmogorov-Smirnov test allows the user to reject a type of probability distribution for the data if the calculated D-value is greater than a threshold value for a given probability of the fit being valid and the number of sample data points. For 64 tests and a 5% level of significance the D-value is 0.17. The Anderson-Darling test is a modified version of the Kolmogorov-Smirnov test that gives more weight to the distribution tails, which can be rejected at the 5% point for values above 2.492 (Johnson 2000). The chi-squared test is another goodness-of-fit test that can be used to reject a type of fit distribution if the value is greater than a threshold value and may be used on discrete distributions (Johnson 2000). The results from these three goodness-of-fit tests are all below their threshold values, indicating that the lognormal distribution provided good agreements with the results of the study. Overall, the correlation coefficients of the lognormal cracking probability distribution fit functions to the stress-to-strength ratio at cracking using the splitting tensile strengths calculated from the compressive strength showed that all of the fit functions were able to be well fit with a lognormal probability density function, with the Raphael fit function showing the highest correlation coefficient.

Discussion

Some of the differences between lognormal distributions fit for different models relating the compressive strength to splitting tensile strength could be because the models were based on data from different sizes of concrete specimens. The splitting tensile tests performed as part of this study were performed on smaller cylinders, 100×200 mm (4×8 in.), compared to those used in the Raphael study, which were cylinders 150 mm (6 in.) in diameter, leading to higher measured values in the current study because of the size effect (Kadlečeck et al. 2002).

The mean concrete measured cracking stress-to-tensile strength value compares well to the expected value of 1.0 when tensile strength reductions of 30% for loading rate and 10% for specimen

Table 16. Comparison of Lognormal Distributions of Concrete Cracking Stress to Tensile Strength as Calculated from the Compressive Strength

Equation source	Test results of this study	Proposed fit function	Raphael fit function (1984)	ACI 318-08 fit function	Carino and Lew fit function (1982)
Fit parameter a	—	0.266	1.7	6.7	1.15
Fit parameter b	—	0.907	0.666	0.5	0.71
Maximum stress-to-splitting tensile strength at cracking	0.79	0.81	0.90	0.89	0.93
Minimum stress-to-splitting tensile strength at cracking	0.37	0.40	0.49	0.51	0.5
Mean, μ	−0.57	−0.57	−0.40	−0.36	−0.37
Standard deviation, σ	0.16	0.16	0.14	0.13	0.14
Correlation coefficient, r^2	0.95	0.84	0.90	0.88	0.89
Kolmogorow-Smirnov GOF D-value	0.087	0.058	0.068	0.083	0.063
Anderson-Darling GOF test value	0.59	0.31	0.30	0.45	0.26
Chi-squared GOF test	4.0	3.56	1.95	2.04	1.73

Note: GOF = goodness of fit.

Table 17. Concrete Cracking Probability versus Cracking Stress to Tensile Strength Ratios for Different Splitting Tensile Strength Fit Functions

Failure probability (%)	Test results of this study	Relationship developed in this study	Raphael (1984)	ACI 318-08, Chapter 18	Carino and Lew (1982)
75	0.64	0.63	0.74	0.79	0.76
50	0.57	0.56	0.67	0.72	0.69
25	0.51	0.51	0.61	0.67	0.63
10	0.46	0.46	0.56	0.62	0.57
5	0.44	0.43	0.54	0.59	0.55

size are considered (Kadlečeck et al. 2002; Emborg 1998b). Starting at a ratio of 1.0 and applying these corrections, this gives an expected mean cracking stress to splitting tensile strength of $1.0 \times 0.70 \times 0.90 = 0.63$, which is close to the measured value of 0.57. The restrained stress experiments described in this study were all conducted with the same size Invar bars. Future work could investigate the effects of the degree of restraint on the cracking probability distribution measured.

For each lognormal distribution described in Table 16, a relative probability of failure may be calculated for different stress-to-tensile strength ratios. Table 17 shows the cracking stress-to-tensile strength ratios for different probabilities of failure. The level of risk that is acceptable is very subjective. Different levels of cracking probability may be determined based on the calculated stress to tensile strength ratio in design. Different risks of cracking may be acceptable in different circumstances. Fig. 10 shows one possible classification system using Raphael's correlation between tensile and compressive strength and 25, 50, and 75% cracking probabilities used to classify low, medium, high, and very high cracking probabilities. Other probability classification systems could be developed using the probability density functions described in this paper.

The high correlation coefficients found for the different probability distributions calculated showed that all of the cracking probability distributions described in Table 16 could be used in a thermal stress analysis, provided that the same corresponding fit function to calculate the splitting tensile strength from the compressive strength is used in the analysis. This means that if the Raphael fit function is used to calculate the splitting tensile strength from the measured compressive strength, the cracking probability distribution calculated using the Raphael fit function should be used to classify the cracking probability. The use of thermal stress cracking

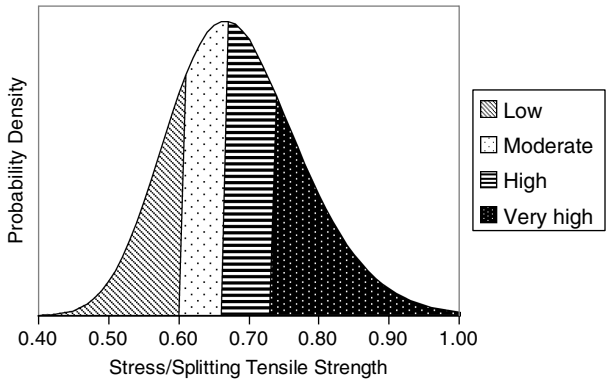

Fig. 10. Cracking probability categories for stress to estimated splitting tensile strength ratios using the Raphael (1984) fit function

probability categories based on the calculated splitting tensile strength from compressive strength tests is particularly suited for use in thermal stress control plans because compressive strength data are more commonly used in concrete mixture qualification and quality control. The standard deviation of the lognormal cracking probability distribution calculated using Eq. (2) from compressive strength data did not change much from that calculated from the measured splitting tensile strength values.

Conclusions

Cracking probability density functions were developed by comparing the tensile stress at cracking in a rigid cracking frame test to the splitting tensile strength of match-cured concrete cylinders. A measured stress-to-measured splitting tensile strength of 0.57 corresponded to a 50% probability of cracking, with a lognormal standard deviation of 0.16. This value compares well with the expected ratio of 1 when reductions in strength for loading rate and specimen size are considered. A lognormal distribution fit the cracking frame stress at cracking to splitting tensile strength ratios well. The Raphael fit function had the best correlation coefficient of the fit functions examined in this study, although all of the fit functions examined performed well. This implies that for design purposes, the concrete tensile strength as calculated from the compressive strength can be used in thermal stress analysis.

Acknowledgments

The authors wish to express their gratitude to the Texas Department of Transportation through Project 0-4563 for funding this research. The work of Jason Meadows at Auburn University in performing some of the rigid cracking frame and concrete mechanical property tests is also gratefully acknowledged. The guidance and assistance of Dr. Rupert Springenschmid and Mr. Erwin Gierlinger to develop the cracking frame test setup are appreciated. Dr. Klaas van Breugel is thanked for providing information on concrete splitting tensile testing performed.

References

American Association of State Highway and Transportation Officials (AASHTO). (2008). "Standard practice for estimating the crack tendency of concrete." *T 334-08*, Washington, DC.

American Concrete Institute (ACI). (2007). "Report on thermal volume change effects on cracking of mass concrete." *ACI 207.2R*, ACI Committee, Detroit.

American Concrete Institute (ACI). (2008). "Building code requirements for structural concrete (ACI 318-08) and commentary." ACI Building Code Committee, Detroit.

Arıoglu, N., Girgin, Z. C., and Arıoglu, E., (2006). "Evaluation of ratio between splitting tensile strength and compressive strength for concretes up to 120 MPa and its application in strength criterion." *ACI Mater. J.*, 103(1), 18–24.

ASTM. (2003). "Standard specification for coal fly ash and raw or calcined natural pozzolan for use in concrete." *C618*, West Conshohocken, PA.

ASTM. (2004). "Standard test method for splitting tensile strength of cylindrical concrete specimens." *C406*, West Conshohocken, PA.

ASTM. (2010). "Standard practice for estimating concrete strength by the maturity method." *C1074*, West Conshohocken, PA.

ASTM. (2011). "Standard Specification for portland cement." *C150*, West Conshohocken, PA.

British Standards Institution (BSI). (2009). "Testing hardened concrete. Tensile splitting strength of test specimens." *EN 12390-6*, London.

Brooks, A. G., Schindler, A. K., and Barnes, R. W. (2007). "Maturity method evaluated for various cementitious materials." *J. Mater. Civ. Eng.*, 10.1061/(ASCE)0899-1561(2007)19:12(1017), 1017–1025.

Carino, N. J., and Lew, H. S. (1982). "Re-examination of the relation between splitting tensile and compressive strength of normal weight concrete." *ACI J.*, 79(3), 214–218.

Davies, J. D., and Bose, D. K. (1968). "Stress distribution in splitting tests." *ACI J.*, 65(8), 662–669.

Eberhardt, M., Lokhorst, S. J., and van Breugel, K. (1994). "On the reliability of temperature differentials as a criterion for the risk of early-age thermal cracking." *Rilem Rep. 25, Thermal cracking in mass concrete*, R. Springenschmid, ed., E & FN Spon, London, 353–360.

Emborg, M. (1998a). "Models and methods for computation of thermal stresses." *Rilem Rep. 15, Prevention of thermal cracking in concrete at early ages*, R. Springenschmid, ed., E & FN Spon, London, 178–230.

Emborg, M. (1998b). "Developing early age mechanical behavior." *Rilem Rep. 15, Prevention of Thermal Cracking in Concrete at Early Ages*, R. Springenschmid, ed., E & FN Spon, London, 76–148.

Gajda, J., and VanGeem, M. (2002). "Controlling temperatures in mass concrete." *Concr. Int.*, 24(1), 58–62.

Hossain, A. B., and Weiss, J. (2004). "Assessing residual stress development and stress relaxation in restrained concrete ring specimens." *Cement Concr. Compos.*, 26(5), 531–540.

Johnson, R. A. (2000). *Miller and Freund's probability and statistics for engineers*, 6th Ed., Prentice Hall, Upper Saddle River, NJ.

Kadlečeck, V., Sr., Modrý, S., and Kadlečeck, V., Jr. (2002). "Size effect of test specimens on tensile splitting strength of concrete: General relation." *Mater. Struct.*, 35(1), 28–34.

Kanda, T., Momose, H., Imamoto, K., and Mihashi, H. (2008). "Stochastic approach to shrinkage cracking control for reinforced concrete structural elements." *J. Adv. Concr. Technol.*, 6(1), 121–133.

Mangold, M. (1998). "Methods for experimental determination of thermal stresses and crack sensitivity in the laboratory." *Rilem Rep. 15, Prevention of Thermal Cracking in Concrete at Early Ages*, R. Springenschmid, ed., E & FN Spon, London, 26–39.

Oluokun, F. A., Burdette, E. G., and Deatherage, J. H. (1991). "Splitting tensile strength and compressive strength relationship at early ages." *ACI Mater. J.*, 88(2), 115–121.

Pijaudier-Cabot, G., Omar, M., Loukili, A., and Pape, Y. L. (2005). "Creep—Damage interaction in concrete structures." *11th Int. Concrete on Fracture*, International Congress on Fracture (ICF), 6.

Raphael, J. M. (1984). "Tensile strength of concrete." *ACI J.*, 81(2), 158–165.

Riding, K. A., Poole, J. L., Schindler, A. K., Juenger, M. C. G., and Folliard, K. J. (2009). "Effects of construction time and coarse aggregate on bridge deck cracking." *ACI Mater. J.*, 106(5), 448–454.

RILEM Technical Committee 119-TCE. (1998). "Adiabatic and semi-adiabatic calorimetry to determine the temperature increase in concrete due to hydration heat of cement." *Rilem Rep. 15, Prevention of thermal cracking in concrete at early ages*, R. Springenschmid, ed., E&FN Spon, London, 315–330.

Rostásy, F. S., Tanabe, T., and Laube, M. (1998). "Assessment of external restraint." *Rilem Rep. 15, Prevention of Thermal Cracking in Concrete at Early Ages*, R. Springenschmid, ed., E & FN Spon, London, 149–177.

Schrage, I., and Summer, T. (1994). "Factors influencing early cracking of high-strength concrete." *Rilem Rep. 25, Thermal Cracking in Mass Concrete*, R. Springenschmid, ed., E & FN Spon, London, 237–243.

Shah, S. P., Swartz, S. E., and Ouyang, C. (1995). *Fracture mechanics of concrete: Applications of fracture mechanics to concrete, rock and other quasi-brittle materials*, Wiley, New York.

Springenschmid, R., and Breitenbücher, R. (1998). "Influence of constituents, mix proportions and temperature on cracking sensitivity of concrete." *Rilem Rep.15, Prevention of Thermal Cracking in Concrete at Early Ages*, R. Springenschmid, ed., E & FN Spon, London, 40–50.

van Breugel, K., and Lokhorst, S. J. (2001). "Stress-based crack criterion as a basis for prevention of through-cracks in concrete structures at early ages." *Early age cracking in cementitious systems*, A. Bentur and K. Kovler, eds., RILEM, Haifa, Israel, 229–236.